SPE/DOE
Society of Petroleum Engineers
U.S. Department of Energy

SPE/DOE 24116

Gravity Stable Displacement of Oil by Hydrocarbon Gas After Waterflooding

O.S. Hustad and Torleif Holt, IKU

SPE Members

This paper was prepared for presentation at the SPE/DOE Eighth Symposium on Enhanced Oil Recovery held in Tulsa, Oklahoma, April 22-24, 1992.

ABSTRACT

This paper presents experimental and simulated results from two vertical core floods. The core floods consisted of injecting equilibrium gas and separator gas from the top of the core after water flooding from the bottom, respectively.

The results show that an oil bank was formed in both experiments. When separator gas was injected, oil was also recovered by vaporization.

Compositional analysis of the produced fluids during separator gas injection shows that considerable amounts of intermediate components were produced as condensate after gas breakthrough. Significant end effects were observed in the final water saturation profiles due to capillary hold-up. Analysis of the final oil saturation in the core indicates a significant gradient due to vaporization, and greater than that modeled by the compositional simulator based on an equation of state.

INTRODUCTION

Water injection into sandstone oil reservoirs may achieve high sweep efficiencies. However, considerable quantities of oil will still remain in a reservoir at the end of a successful water flood, with typically more than 50% of the original oil in place. This residual oil is a target for gas flooding after water flooding, termed here as tertiary gas injection.

Gas injection may recover additional oil because of lower residual oil saturation after gas flooding, typically 5% to 30%. During gas flooding, the oil saturation is reduced due to convective flow and mass exchange between oil and gas.

Besides improving microscopic sweep efficiency, tertiary gas injection may reach regions of a reservoir not swept by water, for example "attic oil." The situation is, however, more often one in which the sweep efficiency is low for tertiary gas injection, a general problem associated with injecting gas. Some means of controlling gas mobility may therefore be aimed at, such as gravity stable gas injection or water alternating gas injection.

During tertiary gas injection, large quantities of mobile water are present in the porous medium, causing a long period of water production prior to the arrival of the oil bank at the producers.

Tertiary gas injection introduces conditions for three phase flow. In parts of the reservoir, three phases may be flowing simultaneously, or oil and gas may flow through paths of water saturations different from connate. This implies that the process may be situated in the three phase space at positions different from those where the relative permeabilities are usually measured. Correlations have been introduced in order to estimate oil relative permeability in the three phase mode from measured two phase data to be applied in reservoir simulators.[1] The correlations are introduced because these quantities are not easily accessible experimentally.

High water saturations in the porous medium may also influence the mass exchange between gas and oil, and thus modify the process efficiency in an unfavorable

References and illustrations at end of paper

way. The rate of mass transfer will be reduced if the components have to diffuse through water barriers. In laboratory core floods, too high injection rates may result in incorrect high residual oil saturations. On a reservoir scale, the microscopic displacement should be less influenced by slow mass transfer. Long range compositional interactions may, however, be reduced by the presence of water.

A large number of laboratory experiments have been performed in order to investigate various aspects related to the effects of water on oil recovery during secondary and tertiary immiscible gas injection. Low residual oil saturations are frequently obtained also in systems where mass transfer between oil and gas is absent.[2-4] Mass transfer of oil components into the flowing gas may improve recovery if the remaining oil is not immobilized due to increased viscosity caused by the loss of light and intermediate components.[5]

Presented below are the results from two gas injection experiments in vertical cores performed under reservoir conditions in one-piece Bentheimer sandstones of 1.2 meters length at low injection rates.[6] The experiments were performed in a gravity stable mode in order to secure a high sweep efficiency. The first experiment, Experiment 1, involved hydrocarbon fluids that were in equilibrium under reservoir conditions. The injection gas was the equilibrium gas to the oil. The purpose of this experiment was to analyze how oil was produced due to convective flow and avoid compositional effects due to mass transfer. The second experiment, Experiment 2, was performed under almost similar conditions as the first experiment. The injection gas was a separator gas and its purpose was to reveal the effects of vaporization.

Relevant capillary pressures, two phase relative permeabilities, zero oil isoperm data, reservoir fluid properties, and fluid properties from the flash processes are also presented.

The first experiment was simulated with a pseudocompositional model[7] to investigate parameters such as capillary pressures, relative permeabilities, and their end point values. The second experiment was simulated, applying rock curves established from the simulation of the first experiment and using the same compositional model with an EOS characterisation having 6 and 24 components.

ROCKS AND FLUIDS

Three cores of Bentheimer sandstone, all from the same block, were used in the experimental work. Their characteristics are summarized in Table 1. Small plugs of the same Bentheimer sandstone block were also used for centrifuge measurements of capillary pressures. All core materials were pretreated in the same manner in order to achieve the same wetting characteristics.

The composition of the artificial formation water used is given in Table 2. The solution contains the most important ions found in the formation water of the reservoir in question. Barium, however, was replaced by strontium in order to avoid precipitation of solids. The formation factors of the water are 1.02187 cm^3/Scm^3 at 92°C and 314 bar, and 1.0255 cm^3/Scm^3 at 99°C and 315 bar.

The displacement experiments were performed with live oil from a North Sea oil reservoir. The live oil was recombined from known separator production rates. An equilibrium gas-oil system was established by adding separator gas to the recombined oil until a two phase system was formed with desired phase volumes at 91.9°C and 313.5 bar. The oil and gas phases were then separated into separate cells. A pressure-Volume diagram was generated for the oil to ensure its saturation pressure of 313.5 bar at 91.9°C. The compositions and properties of the hydrocarbon fluids used in the displacement experiments are given in Table 3 as characterized by gas chromatography (GC). The molecular weight distribution was estimated.

Interfacial tensions (IFT) between equilibrium gas and oil, and between equilibrium oil and water were measured by the pendant drop technique in a visual high pressure cell. With respect to the measurements performed with the gas-oil equilibrium system, it was impossible to keep the drop permanently hanging due to the low interfacial tension in the system. The experiment was therefore recorded on video, and the picture giving the most characteristic "drop shape" was measured following the standard procedure for the method. Where the oil-water system was concerned, the oil drop behaved normally.

Two Soave-Redlich-Kwong (SRK) EOS characterizations consisting of 6 and 24 components were constructed to model a single stage flash from reservoir conditions to standard conditions.[6]

The individual hydrocarbons were assumed and assigned equal molecular weights in the stock tank oil (STO) and condensate. The condensate's C_{48+} fraction molecular weight was also assumed equal to the STO's C_{48+} fraction. Due to the small quantities of condensate C_{48+}, this approximation is considered reasonable for estimating the overall compositions.

The established SRK EOS characterizations, and their pseudocomponents, are given in Tables 4 and 5 for the 6 and 24 component systems, respectively. When the compositions from Table 3 are grouped in this manner, there are discrepancies in the pseudocomponent molecular weights under reservoir conditions between the two equilibrium hydrocarbon

phases. These discrepancies are greatest (approximately 30%) for the heaviest pseudocomponent in the 6 component characterization, C_{29+} fraction. The pseudocomponent molecular weights for the 24 component system deviated at most by 1.3%. The oil phase molecular weights were used in both fluid models.

These characterizations reproduced most of the measured experimental data within the range of expected experimental error. Two weaknesses were, however, observed. First, the saturation pressure of equilibrium gas was too high, 350 and 333 bar for the 6 and 24 component models, respectively. Secondly, the condensate density from the equilibrium gas was too low by 7.2% and 12.2% for the 6 and 24 component models, respectively.

RELATIVE PERMEABILITIES

The apparatus used for measuring relative permeabilities by the steady state method is shown in Fig. 1. The apparatus has feed lines for water, oil and gas. The gas rate was controlled by a mass flow controller. Water and oil were delivered by HPLC-pumps. The fluids were mixed prior to the core entrance. Water and oil were recycled, whereas the gas was transported through the system and exited via a cooled liquid trap and a bubble flow meter. The measurements were made at room temperature (21°C), and the separator pressure was kept at 7 bar. Decane was used as oil and nitrogen as gas. The total flow rate during the measurements was approximately 5 cm^3/min at separator pressure.

The experiments always started with the core being 100% saturated with artificial formation water. Decane was then injected to establish the irreducible water saturation, S_{wir}. For measurements of two phase relative permeabilities, oil and water, or gas and oil were injected at pre-determined ratios. When a steady state was established, differential pressure, separator levels and separator mass were recorded before a new fluid ratio was initiated.

Steady state measured relative permeability values and simulator relative permeability curves for the oil-water and the gas-oil systems are shown in Figs. 2 and 3, respectively. The curves in the two figures are valid for drainage processes, i.e. decreasing water saturation and increasing gas saturation. Fig. 2 includes both imbibition and drainage experimental water relative permeabilities. Fig. 3 also includes gas permeabilities measured in three phase mode. These were measured for a process path corresponding to Experiment 1.

During the measurement of gas-oil relative permeabilities, the water saturation (S_{wir}) was reduced from 17.7% to 13.2%. An average irreducible water saturation of 14.5% was determined from repeated measurements of the irreducible water saturation for the oil-water system. The irreducible water saturation was always reduced when gas entered the core and was lowest at residual oil, S_{org}. The measured residual oil saturations were 38.4% (S_{orw}) and 27.7% (S_{org}); see Fig. 4.

Measurements of "zero oil isoperms" in the three phase space were initiated at residual oil saturations for the oil-water system, S_{orw}. Gas and water were first injected with a low gas/water ratio until steady state was reached. After the necessary data was recorded, 0.5 cm^3/min decane was injected together with water and gas until a new steady state was obtained. Then a higher gas/water ratio was injected, and the same procedure was repeated for various gas/water ratios as indicated by the arrows in Fig. 4.

The data points obtained for no oil flow lie on a typical concave isoperm as viewed for the oil apex, but cover only a limited range of gas saturations.

Measurements were also made for processes where the three phase space was entered through S_{wir}. The points of no oil flow were distributed differently compared to those entering at S_{orw}.[6] The results obtained thus indicate that the points of no oil flow are process dependent, which has also been observed by others.[8]

The measurements of three phase relative permeabilities also demonstrated that rather low oil saturations are obtainable with a high interfacial tension (nitrogen-decane). As these saturations virtually are lower than the saturation obtained during the high pressure equilibrium gas injection, it is believed that IFT effects have only minor impact on residual oil saturations during the tertiary gas displacement experiments and during the steady state relative permeability experiments presented here.

The Appendix outlines the modifications to the relative permeability correlation of Stone[9] used to simulate Experiments 1 and 2, described below. The correlation exponent value, n, was equal to 4, for both experiments. Also outlined is the procedure by which the water saturation was transformed between block and rock curve values. The two phase relative permeability data were not altered due to changes in IFT.[10]

CAPILLARY PRESSURES

The oil-water and gas-oil capillary pressure rock curves used in the simulations are shown in Fig. 5 along with the experimental values obtained from centrifuge measurements.[6] Four sets of capillary pressure data have been measured:

1. Decane drained by air to $S_{or} \approx 5.3\%$ (IFT of 23.4

mN/m). No water was present.
2. Water drained by decane to $S_{wir} \simeq 13.2\%$ (IFT of 37.1 mN/m).
3. Water drained by decane to $S_{wir} \simeq 16.5\%$ and thereafter drained by air to $S_{wir} \simeq 0.5\%$ and $S_{org} \simeq 4.5\%$.
4. Water drained by air to $S_{wir} \simeq 4.5\%$ (IFT of 72.0 mN/m).

The results from the capillary pressure measurements conclude that the liquid residual saturations are much lower when gas is present. The irreducible water saturation is highest when displaced by oil only. When gas is introduced, the liquid residual saturations become significantly lower.

FLOODING EXPERIMENTS

Apparatus

The displacement experiments were performed in a high pressure flooding apparatus as schematically shown in Fig. 6. In Experiment 2, the gasometers were replaced by a gas collection container with pressure detector. A back pressure valve before the inlet of the container secured a pressure of one atmosphere in the separator tubes.

The injection fluids were stored in one liter piston bottles. These fluids were injected into the cores by pumping paraffin into the hydraulic side with the use of a positive displacement pump. The core holder and the oil and gas bottles were kept inside the oven. The high pressure line and the back pressure valve, located outside the oven, were heated in order to avoid the formation of gas hydrates. The effluent from the back pressure valve was led to the separator in order to collect produced oil and water. The gas flow then continued to the gas collection system. The separator consisted of two exchangeable graduated glass tubes with neoprene septa. The back pressure valve effluent was led to the desired tube and gasometer by use of time controlled valves. Samples of the produced gas were taken at given intervals and analyzed by GC. The collected oil samples were characterized by composition, density and average molecular weight.[6]

The production histories were observed and recorded by use of a high pressure sapphire tube, located just behind the core exit, and a video recording system.

Experimental Procedure

An outline of the flooding sequences is given in Table 6. The experiments were performed at 92°C and 314 bar in the case of Experiment 1, and at 99°C and 315 bar in the case of Experiment 2.

The cores were vertically mounted in the core holder and initialized with 100% water saturation. Reservoir oil was injected through the top of the core holder at variable injection rates. Water was then injected from below. Finally, gas was injected through the top of the core holder.

During the oil and water injection, produced fluids were collected in a separator at standard conditions. Some water was caught in the oil phase as small droplets or emulsion during these steps. The oil phase in the separator was therefore always analyzed for water by the Karl Fischer technique. During gas injection, fluid was sampled and analyzed as described above.

At the end of each core flood the core was cooled and depressurized. The core was then taken out of the core holder and cut in pieces of approximately 10 cm length. Each piece was then extracted by methanol and toluene. The water content of each core piece was determined by Karl Fisher water analyses. The toluene extracts were taken to "dryness," and the evaporation residue determined gravimetrically. The amount of degassed oil in each core piece was determined by weighing before extraction, and subtracting the weight of the water content and the weight of the cleaned and dried core piece.

For Experiment 1, the core was cooled to -20°C before depressurizing. This resulted in leakage of hydraulic oil into the core which made determination of oil saturation profiles impossible. For Experiment 2, the core was depressurized at room temperature, through the top of the core, at a slow pace (three days), thus preventing disturbance of the saturation profiles. The core was then taken out of the core holder and cooled to -20°C, always keeping the core in a vertical position. Then the sleeve and diffusion barrier were removed and the core divided into pieces.

Simulation Procedure

The simulations of the core flood experiments were performed using an IMPES type compositional simulator.[7]

A one-dimensional grid with 30 grid blocks was constructed to match Experiment 1. 28 of these blocks represented the core, and two blocks, one on each end of the grid, represented the dead end volumes above and below the core.

The two end point blocks had their capillary pressures set to zero along with all residual saturations. The two phase relative permeabilities were modeled with straight lines.

The rock curve minimum residual oil saturation, S_{om}, was set to 15.5% which is lower than both the residual oil saturation for the oil-water system (S_{orw} = 38.4%), and gas-oil system at S_{wir} of 14.5% (S_{org} = 23.8%). The critical gas saturation was zero.

The modified first model of Stone, see Appendix, was applied to the oil relative permeability in the three phase space. The maximum block gas saturation, S_g^{mx}, was set to 95.5%, implying a minimum irreducible water saturation, S_{wir}^g, of 4.5% as measured by the air-water centrifuge measurements. The block oil-water irreducible water saturation, S_{wir}^o, was adjusted to 6.5% in order to achieve a match of the water production in Experiment 1. These values correspond to a block residual oil saturation, S_{org}, of 30% and block irreducible water saturation of 8.3% at the maximum block gas saturation of 61.7%, the gas saturation being fixed by the two phase gas-oil relative permeabilities representing no oil flow. This value is also slightly higher than the measured maximum gas saturation value of 59.1% determined from the gas-oil relative permeabilities.[6]

The rock capillary pressure curves were scaled by the ratio of reservoir/standard condition IFT values. The water saturation transformation described in the Appendix was also applied to the oil-water capillary curve.

The oil flood from the top, and the water flood from the bottom of the core, were simulated to establish the initial saturations prior to the gas flooding. An end effect was observed with regards to water saturation after oil flooding. The residual oil saturation, S_{orw}, was evenly distributed in the blocks with no end effects after water flooding.

A three pseudocomponent fluid model based on an explicit solution scheme was constructed for modeling Experiment 1.[7] The fluid model was constructed from laboratory flash data of equilibrium oil and gas. The model reproduced the laboratory flash results. The model assumes that the phase properties under reservoir conditions are more or less constant due to the insignificant pressure variations during the flooding process, and that the process occurs along one tie line. The fluid K-values and densities at standard conditions assume a linear relationship between the two extreme states (i.e. flash of equilibrium oil and gas). These properties were made dependent on the well stream heavy pseudocomponent.

Simulation of Experiments 1 and 2 applied the same rock curves. Experiment 2 was simulated with the two EOS fluid models described above.

EXPERIMENT 1

The recoveries at standard conditions from Experiment 1 are shown in Fig. 7. The markers indicate the experimental values and the lines indicate the simulation results. Water production starts instantly as gas is injected. Water production shows a reduction in rates when oil and gas break through. Continued water production was observed as long as gas was injected.

The oil recovery, shown as total oil produced, also showed a reduction in rate after the breakthrough of gas. The initial STO produced from the oil bank was thicker than the equilibrium oil's STO. This indicates that the water flood had absorbed some of the lighter hydrocarbon components from the equilibrium oil. This is not accounted for in the simulations.

Breakthrough of oil and gas occurred at 0.324 and 0.469 pore volume gas injected (PVI), respectively. This was determined from video recordings of the core effluents. The simulated recoveries matched the experimental values well. There is a slight deviation in gas recovery. This is believed to be partly due to error in the experimental measurements of the produced gas and the flash data of equilibrium gas.

The final water saturations, see Fig. 8, obtained by experimental measurements and simulation correspond well but are by no means perfect. The simulation shows that the residual water saturation was never reached, due to capillary end effects and residual saturations. The 1.2 meter core may also be too short to precisely determine how low the water saturation may become due to convective flow. The lowest water saturation in the uppermost part of the core was measured at 11.2%.

Simulations using the three phase relative permeability to gas were also made. The recoveries proved insensitive to the choice of gas relative permeabilities.

The 24 component EOS model was also used to simulate Experiment 1 after a match was obtained. The equilibrium oil's gas compositions were used as the injection gas. The recoveries were practically identical.

Simulations were also made with 112 blocks representing the core. To maintain a match of the water recovery, the maximum irreducible water saturation, S_{wir}^o, had to be increased to 8.0%. This adjustment had little influence on the oil recovery. However, it reveals that the irreducible water saturation is also dependent on the number of grid blocks.

EXPERIMENT 2

The separator gas injection flood was performed at a temperature 6.5°C higher than the equilibrium gas injection flood. The reasons for choosing this temperature relate to other flooding experiments performed earlier under these conditions in shorter Bentheimer and Berea cores.[6] It is assumed that the EOS parameters also apply at this temperature.

The simulator rock curves were fixed as in Experiment 1, and the capillary pressures were not permitted to vary with varying IFT. This approximation of the rock curves should give optimistic recoveries since capillary hold-up of oil is not introduced due to increasing IFT caused by vaporization behind the gas-oil front.

Fig. 9 shows the recoveries obtained by Experiment 2 and the simulated results using the two EOS fluid models. The oil and gas breakthrough times as recorded by video were 0.342 and 0.477 PVI, respectively.

The oil recovery from the 6 component system resembles the experimental oil recovery more closely than the 24 component system which is more pessimistic.

The water and gas recoveries are practically the same for the two fluid models. Compared to experimental data, the simulated gas recoveries are lower than the experimental values right after gas breakthrough, but become higher as more gas is injected. This indicates that the fluid models together with the rock curves do not represent the convective flow, vaporization and flash process correctly. The simulated water production more or less tends to stop after 0.8 PVI, whereas the experimental results do not. For some reason not clearly understood, the oil-water capillary pressure curve, together with the residual saturations in the simulator, lock the water in place.

The simulated water saturations at the end of the gas flooding are shown in Fig. 8. The simulations produced different results, which is caused by a locking effect due to the oil phase reaching different residual saturation values causing no oil flow. These water saturation profiles were not observed in earlier simulations when the irreducible water saturation was constant and not dependent on the gas saturation.[6] In fact, the previous simulations had very similar water saturation profiles as in Experiment 1. The experimental water saturation in the uppermost region of the core was measured at 8.3%.

As may also be seen, the water recovery is greater for this experiment compared to Experiment 1, see Figs. 7 and 9. One explanation may be that, as oil is vaporized, it makes pore space available for immobile water to flow, reducing the water saturation further. This reasoning also lies behind the suggested gas dependent irreducible water saturation formulation outlined in the Appendix. Precautions should however be taken as to the choice of residual saturations. The water saturation after 1.7 PVI is 2.2% lower in Experiment 2 compared to Experiment 1.

The final core oil saturation profile from the flooding experiments (see Fig. 10) shows that the oil saturation gradient in the simulated results is smaller than the gradient estimated from experimental results. The measured experimental results have been scaled by the oil's initial B_o/ρ_o^s factor. This factor is reduced when the oil undergoes vaporization, i.e. it becomes less volatile. Hence, the estimated experimental oil saturations and saturation gradient in the core are conservative. That is, the saturations are too high and the saturation variation between the inlet and outlet should be greater.

The oil extracts from separate core pieces were dried, and the masses of these evaporation residuals were measured. Results show that the heavy components were evenly distributed within the core, implying that the oil saturation gradient is mainly due to vaporization.

Different oil saturation profiles are modeled by the 6 and 24 component systems. This difference is mainly due to how the EOS models the vaporization process.[6] Since the rock curves are the same in both models, the fluid characterization is important when trying to model the vaporization process; and, as can be seen, the fluid model has a significant influence on how the oil saturations are modeled. The 6 component model final oil saturation was 8.6% and the 24 component model final oil saturation was 6.0%.

The mixing due to convective flow, the vaporization process, and the flash calculations, cause the oil recoveries to be different. This difference, in addition to convective flow and vaporization, is caused by the flash of the fluids from reservoir to standard conditions.

The compositions of the produced fluids have been measured to show how the vaporization process affects the compositions of the produced fluids.[6] The simulations reproduced the lighter components' compositions rather well.

The C_{16+} oil weight fractions are illustrated in Fig. 11. Due to small fluid volumes, little compositional data is available prior to gas breakthrough. However, the simulated oil compositions tend to resemble the experimental results prior to 1.5 PVI. The simulated concentrations thereafter flatten out, in contrast to the experimental values which continue to increase. An explanation for this is that the process has vaporized to an overall composition that lies on a "limiting" tie line in the 6 component EOS model.

Fig. 12 shows the produced oil's C_{22+} weight fractions. The 24 component model reproduces the experimental results much better than the C_{16+}

fractions from the 6 component model, in contrast to the recovery curves.

The simulated oil compositions between 0.9 and 1.4 PVI have a sudden jump in value due to a hold-up of oil causing no flow out of the core, as may also be seen in Fig. 9 by the flattening of the oil recovery curve. This artifact implies that the rock curves that describe convective flow have a significant influence on the compositions produced.

DISCUSSION

Reproducing the results from Experiment 1 using a simulator proved not to be a simple task, especially with respect to water recovery. The work was very time consuming. The use of relative permeabilities and capillary pressure curves along with their residual saturations have resulted in a satisfactory match of convective flow in Experiment 1. However, introducing the vaporization mechanism of Experiment 2 increases the complexity of the process, and this has not been successfully simulated here.

Fig. 13 shows the oil production from Experiments 1 and 2. The total oil recovery from Experiment 1 is also represented by two other curves, STO production from equilibrium oil due to convective flow and condensate production from the equilibrium gas. These recovery curves were deduced from the flash data of the equilibrium fluids, total gas and oil recoveries, and gas/oil ratios.

As may be seen, the oil production from Experiment 2 is considerably higher than that due to convective flow from Experiment 1. At 1.7 PVI, approximately 60% more oil was produced through Experiment 2. This illustrates, for this system, the extraction of oil components into the flowing gas phase is a significant mechanism for oil recovery during gravity stable tertiary displacement of oil by gas after water injection.

CONCLUSIONS

The objectives were to describe how conductivity (relative permeability), capillary forces (capillary pressure) and component exchange between flowing oil and gas influence the recovery of oil during gravity stable gas injection after water flooding. The following conclusions may be drawn from this work.

1. Both convective flow through the formation of an oil bank and thus vaporization are important mechanisms contributing to additional oil recovery during tertiary gravity stable gas flooding.

2. The experimental core oil saturation was reduced from 38% after water flooding, to 22% after flooding with 1.7 PV of equilibrium gas. Flooding with separator gas reduced the experimental oil saturation below 13% after 1.7 PVI and further below 10% after 3.4 PVI.

3. End effects during laboratory core floods have a strong effect on the water production history and final water saturation distribution. The end effects must be accounted for in the simulations in order to get a correct picture of the laboratory scale recovery process.

4. Measurements of three phase relative permeabilities for oil demonstrate that the process path significantly influences the results obtained, and the simulations show that the oil isoperms strongly influence the oil recovery. A simple modification of Stone's first model was adequate for matching the oil recovery.

5. Caution should be exercised when using the EOS to model the vaporization process. The 6 component characterization had both a higher oil recovery and higher final oil saturation compared to the 24 component characterization.

6. The final oil saturation profile in Experiment 2 was best reproduced by the 24 component fluid model. However, the oil recovery was less precisely reproduced with this model.

7. The final oil saturation gradient with respect to position in the core is mainly due to vaporization. This gradient as modeled by the EOS was smaller than that measured experimentally.

8. The irreducible water saturation determined experimentally by the steady state flow experiment proved to be too high when compared to the final core saturations in the upper part of the cores and seem dependent on gas saturation. The simulator irreducible water saturation shows also a dependency on the number of grid blocks.

NOMENCLATURE

B_o - Oil formation volume factor (cm^3/Scm^3)
k_{rocw} - Maximum relative permeability to oil at S_{wir} and zero gas saturation
k_{row} - Relative permeability to oil for oil-water system
k_{rog} - Relative permeability to oil for gas-oil system
MW - Molecular weight
p_c - Critical pressure
S_{gc} - Critical gas saturation
S_{wir} - Irreducible water saturation
S_{orw} - Residual oil saturation for oil-water system
S_{org} - Residual oil saturation for gas-oil system with irreducible water saturation
S_{om} - Minimum oil saturation in three phase saturation space
S_j^* - Normalized saturation of phase j
T_c - Critical temperature

V_c - Critical volume
ρ_j - Mass density of phase j

Subscripts

g - Gas
o - Oil
w - Water

Superscripts

b - Block
g - Gas-water system (no oil)
mx - Maximum
n - Oil rel.perm. correlation exponent
o - Oil-water system (no gas)
t - Table or rock curve

ACKNOWLEDGMENTS

The authors gratefully acknowledge the support of Anne-Grethe Hansen in the preparation of this paper. The funding for this work was provided by The Norwegian State R&D Programme for Improved Oil Recovery and Reservoir Technology (SPOR). Additional financing for the preparation of this paper was provided by NTNF. Their financial support is gratefully acknowledged.

REFERENCES

1. BAKER, L.E.: "Three-Phase Relative Permeability Correlations." Paper SPE 17369 presented at the 1988 SPE/DOE Symposium on Enhanced Oil Recovery, Tulsa, April 17-20.

2. DULLIEN, F.A.L., CATALAN, L., CHATZIS, I. and COLLINS, A.: "The Effect of Wettability and Heterogeneities on the Recovery of Waterflood Residual Oil with Low Pressure Inert Gas Injection, Assisted by Gravity Drainage." Proc. 6th European Symposium on IOR, Stavanger (1991) 695-704.

3. NAYLOR, P. and FRØRUP, M.: "Gravity-Stable Nitrogen Displacement of Oil." Paper SPE 19641 presented at the 64th Annual Technical Conference and Exhibition, San Antonio (Oct. 8-11, 1989).

4. NECTOUX, A.: "Equilibrium Gas Oil Drainage: Velocity, Gravitational and Compositional Effects." Proc. 4th European Symposium on EOR, Hamburg (1987) 779-789.

5. NIKO, H., SCHULTE, A.M., DROHM, J.K. and COTTRELL, C.W.: "The Feasibility of Tertiary Nitrogen Injection in Waterflooded Volatile Oil Reservoirs in the North Sea." Proc. 4th European Symposium on EOR, Hamburg (Oct. 27-29, 1987) 779-789.

6. HUSTAD, O.S., HOLT, T. and HANSEN, A. G.: "Gravity-Stable Displacement of Oil by Hydrocarbon Gas After Water Flooding." IKU report no. 34.2884.00/01/91, Trondheim (Nov. 1991).

7. HUSTAD, O.S. and DALEN, V.: "An Explicit Phase Behavior Model for Pseudocompositional Reservoir Simulation." Paper SPE 19806 presented at the 64th Annual Technical Conference and Exhibition, San Antonio (Oct. 8-11, 1989).

8. OAK, M.J., BAKER, L.E. and THOMAS, D.C.: "Three-Phase Relative Permeability of Berea Sandstone." JPT (Aug. 1990), 1054-1061.

9. STONE, H.L.: "Probability Model for Estimating Three-Phase Relative Permeability." JPT (Feb. 1970) 22, 214-218; Trans., AIME, 249, 214-218.

10. DELCLAUD, J., ROCHON, J. and NECTOUX, A.: "Investigation of Gas/Oil Relative Permeabilities: High-Permeability Oil Reservoir Application." Paper SPE 16966 presented at the 62nd Annual Technical Conference and Exhibition, Dallas (Sept. 27-30 1987).

11. STONE, H.L.:"Estimation of Three-Phase Relative Permeability and Residual Oil Data." J.Can.Pet.Tech., v.12, No. 4 (Oct.-Dec. 1973), 53-61.

12. LOHRENZ, J., BRAY, B.G. and CLARK, C.R.: "Calculating Viscosities of Reservoir Fluids From Their Compositions." JPT (Oct. 1964) 1171-1176.

APPENDIX

Three Phase Relative Permeability Correlation

Simulation of the equilibrium gas injection flooding experiment were attempted using Stone's correlations[9,11] for oil phase relative permeability. These correlations either overestimated or underestimated the oil recovery of Experiment 1. This inadequacy was overcome by modifying Stone's first model by the introduction of an exponent term, n, to the normalized saturations represented by the β parameter, as follows:

$$k_{ro} = \frac{k_{row}(S_w)\, k_{rog}(S_g)}{k_{rocw}} \beta^n$$

where

$$\beta = \frac{S_o^*}{(1-S_w^*)(1-S_g^*)},$$

$$S_o^* = \frac{S_o - S_{om}}{1 - S_{wir} - S_{om} - S_{gc}},$$

$$S_g^* = \frac{S_g - S_{gc}}{1 - S_{wir} - S_{om} - S_{gc}},$$

and

$$S_w^* = \frac{S_w - S_{wir}}{1 - S_{wir} - S_{om} - S_{gc}} .$$

The β term may be interpreted as a variable that varies between zero and one for low and high oil saturations, respectively. If the exponent η is one, the correlation is identical to Stone's first model. Increasing n above unity causes the oil isoperms at low values to spread within the saturation space. Decreasing n below unity has the opposite effect.

Values of n above unity also cause the low oil isoperms to become more linear between the two phase values as recommended by Baker.[1]

The block irreducible water saturation was also made dependent on the gas saturation, causing a transformation of the water saturation between the block values and the rock curves. The block irreducible water saturation was modeled by

$$S_{wir}^b = \left[S_{wir}^o \, (S_g^{mx} - S_g^b) + S_{wir}^g \, S_g^b\right] / \, S_g^{mx}$$

where

$$S_g^{mx} = 1 - S_{wir}^g ,$$

and S_{wir}^o and S_{wir}^g are input parameters.

The transformation of block water saturation to rock curve values is

$$S_w^t = S_{wir}^t + \frac{(1 - S_{wir}^t)\,(S_w^b - S_{wir}^b)}{(1 - S_{wir}^b)} .$$

Note that when the irreducible water saturation is made dependent on the gas saturation, the residual oil saturation, S_{org}, is also dependent on the gas saturation; that is to say, $S_{org} + S_{wir}$ is constant.

TABLE 1 - Characteristics of core material.

Length (cm)	Diameter (cm)	Pore vol. (cm^3)	Porosity (%)	Permeability (μm^2)	Use
122.6	3.78	312.8	22.7	2.566	Exp. 1
122.1	3.77	317.2	23.3	2.645	Exp. 2
61.9	3.77	156.9	22.7	2.467	Rel.perm.

TABLE 2 - Composition of artificial formation water.

Component	Concentration	
	(mg/dm^3)	($mmol/dm^3$)
NaCl	22 330	382.1
KCl	382	5.12
NH_4Cl	102	1.91
NaF	3	0.071
$NaHCO_3$	422	5.02
$CaCl_2$	837	7.54
$FeCl_2$	0.26	0.002
$MgCl_2$	207	2.17
$MnCl_2$	0.6	0.005
$SrCl_2$	82	0.516
$B(OH)_3$	301	4.87
$AlCl_3$	0.95	0.007
Total	24 667.81	409.331

TABLE 3 - Experimental flash data from recombined hydrocarbon fluids.

		Experiment 1				Experiment 2		
		Equilibrium Oil		Equilibrium Gas		Oil		Inj. Gas
Comp.	Molecular Weight	Gas Mole %	Oil (STO) Weight %	Gas Mole %	Condensate Weight %	Gas Mole %	Oil (STO) Weight %	Gas Mole %
N_2	28.02	1.202	0.00	1.700	0.00	1.467	0.0	1.762
C_1	16.04	72.350	0.00	79.471	0.00	0.693	0.0	0.714
CO_2	44.01	0.737	0.00	0.651	0.00	71.461	0.0	80.218
C_2	30.07	11.359	0.00	8.582	0.00	10.793	0.03	9.053
C_3	44.09	7.873	0.03	4.971	0.03	8.244	0.21	4.945
i-C_4	58.12	1.014	0.03	0.611	0.04	1.129	0.12	0.544
n-C_4	58.12	2.848	0.18	1.655	0.19	3.203	0.53	1.406
i-C_5	72.15	0.693	0.22	0.444	0.25	0.793	0.45	0.309
n-C_5	72.15	0.880	0.43	0.605	0.52	1.016	0.81	0.396
C_6	86.17	0.590	1.23	0.573	2.05	0.711	1.90	0.294
C_7	91.62	0.418	2.96	0.598	6.09	0.446	4.04	0.359
C_8	104.53	0.0357	4.54	0.139	11.41	0.04351	5.05	
C_9	118.84		4.26		12.26		4.94	
C_{10}	134.0		3.76		11.14		4.54	
C_{11}	147.0		3.42		8.86		3.83	
C_{12}	161.0		3.18		7.46		3.45	
C_{13}	175.0		3.35		6.94		3.67	
C_{14}	190.0		3.25		5.82		3.37	
C_{15}	206.0		3.67		5.62		3.41	
C_{16}	222.0		3.16		4.14		3.20	
C_{17}	237.0		2.55		3.27		2.96	
C_{18}	251.0		3.07		3.18		3.23	
C_{19}	263.0		2.83		2.82		2.99	
C_{20}	275.0		2.50		2.06		2.44	
C_{21}	291.0		2.14		1.78		2.50	
C_{22}	300.0		2.14		1.53		2.05	
C_{23}	312.0		1.66		0.49		1.42	
C_{24}	324.0		1.55		0.39		1.33	
C_{25}	337.0		1.50		0.30		1.28	
C_{26}	349.0		1.46		0.24		1.25	
C_{27}	360.0		1.28		0.16		1.09	
C_{28}	372.0		1.42		0.15		1.21	
C_{29}	382.0		1.47		0.14		1.26	
C_{30}	394.0		1.52		0.11		1.30	
C_{31}	404.0		1.25		0.079		1.07	
C_{32}	415.0		1.05		0.052		0.90	
C_{33}	426.0		1.07		0.039		0.92	
C_{34}	437.0		0.98		0.036		0.84	
C_{35}	445.0		1.00		0.043		0.86	
C_{36}	456.0		0.88		0.049		0.75	
C_{37}	464.0		0.90		0.079		0.77	
C_{38}	475.0		0.72		0.059		0.62	
C_{39}	484.0		0.68		0.022		0.58	
C_{40}	495.0		0.61		0.016		0.52	
C_{41}	502.0		0.54		0.020		0.46	
C_{42}	512.0		0.50		0.020		0.43	
C_{43}	521.0		0.41		0.013		0.35	
C_{44}	531.0		0.35		0.007		0.30	
C_{45}	539.0		0.29		0.003		0.25	
C_{46}	548.0		0.24		0.002		0.21	
C_{47}	557.0		0.19		0.001		0.16	
C_{48+}	791.5		23.58		0.010		20.15	
MW (g/mole)		-	226	-	159	-	205	
Density (g/cm^3)		9.922E-4	0.8485	9.111E-4	0.8033	1.013E-4	0.845	
Formation Volume Factor (cm^3/Scm^3)		1.62		18.0		1.61		
Gas/Oil Ratio (Scm^3/Scm^3)		200.9		4341.63		204.1		
Saturation Temperature (°C)		91.9		91.9		98.4		
Saturation Pressure (bar)		313.5		313.5		275.1		
Saturation Density (g/cm^3)		0.6468		0.2644		0.6532		
Viscosity (cp)		0.43		-		-		
Interfacial tension (mN/m)		1.2						

Interfacial tension between artificial formation water and the equilibrium oil at 313.5 bar and 91.9°C is 21.6 mN/m.

The standard conditions are 1 bar and 15°C.

TABLE 4 - 6 component system's Soave-Redlich-Kwong EOS parameters.

Comp. no.	Comp. ID.	Components	Eq. oil (Mole Frac.)	MW (g/mole)	p_c (Bar)	V_c (cm^3/mole)	T_c (°C)	Acentric Factor
1	HC1	N_2+C_1	0.51639	16.236	46.000	85.93	-82.98	0.0078
2	HC2	$CO_2+C_2+C_3$	0.14067	36.139	46.280	150.22	61.31	0.1349
3	HC5	$C_4+C_5+C_6$	0.06116	68.592	34.000	278.24	181.97	0.2380
4	HC9	$C_7+\ldots+C_{15}$	0.16916	135.992	25.560	460.17	292.72	0.5913
5	HC21	$C_{16}+\ldots+C_{28}$	0.06848	279.089	15.240	1045.56	493.45	1.0133
6	HC40	$C_{29}+$	0.04414	607.199	13.190	1548.19	709.28	1.2781

All binary interaction parameters are zero.

Coefficients for Lohrenz-Bray-Clark viscosity correlation[12]

A0 = 0.1023000
A1 = 0.0233640
A2 = 0.0585330
A3 = -.0407580
A4 = 0.0127642

TABLE 5 - 24 component system's Soave-Redlich-Kwong EOS parameters.

Comp. no.	Comp. ID.	Components	Eq. oil (Mole Frac.)	MW (g/mole)	p_c (Bar)	V_c (cm^3/mole)	T_c (°C)	Acentric Factor
1	N2	N_2	8.438934E-03	28.020	33.940	89.89	-146.95	0.0400
2	CO2	CO_2	5.174288E-03	44.010	73.760	93.96	31.05	0.2250
3	C1	C_1	5.079508E-01	16.040	46.000	99.25	-82.55	0.0085
4	C2	C_2	7.974863E-02	30.070	48.840	147.92	32.25	0.0980
5	C3	C_3	5.575137E-02	44.090	42.460	202.89	96.65	0.1520
6	IC4	$i-C_4$	7.480927E-03	58.120	36.480	262.71	134.95	0.1760
7	C4	$n-C_4$	2.216643E-02	58.120	38.000	254.73	152.05	0.2075
8	IC5	$i-C_5$	7.003191E-03	72.150	33.840	305.84	187.25	0.2528
9	C5	$n-C_5$	1.035671E-02	72.150	33.740	304.04	196.45	0.2543
10	C6	C_6	1.414991E-02	86.170	29.690	370.14	234.25	0.2658
11	HC7	C_7	2.558556E-02	91.620	34.150	321.86	255.65	0.3465
12	HC8	C_8	3.070130E-02	104.530	30.640	374.72	279.22	0.4189
13	HC9	C_9	2.513221E-02	118.840	27.310	437.30	301.41	0.5315
14	HC11	$C_{10}+C_{11}+C_{12}$	4.983222E-02	145.758	22.820	557.21	338.59	0.6611
15	HC13	$C_{13}+C_{14}$	2.541378E-02	182.078	19.510	694.39	378.62	0.7627
16	HC16	$C_{15}+C_{16}$	2.247029E-02	213.106	17.690	802.69	409.99	0.8139
17	HC18	$C_{17}+C_{18}+C_{19}$	2.366305E-02	250.363	16.380	908.74	442.97	0.9365
18	HC20	$C_{20}+C_{21}$	1.152959E-02	282.155	15.620	990.47	471.16	1.0209
19	HC23	$C_{22}+C_{23}+C_{24}$	1.208553E-02	310.364	15.020	1056.10	490.00	1.0724
20	HC26	$C_{25}+\ldots+C_{28}$	1.122273E-02	353.591	14.470	1139.34	520.00	1.1495
21	HC30	$C_{29}+\ldots+C_{32}$	9.345896E-03	396.843	14.030	1204.70	540.00	1.2693
22	HC35	$C_{33}+\ldots+C_{38}$	8.684434E-03	448.059	13.720	1262.22	560.00	1.3475
23	HC42	$C_{39}+\ldots+C_{47}$	5.225152E-03	511.222	13.500	1313.59	580.00	1.4641
24	HC57	$C_{48}+$	2.088703E-02	791.500	13.460	1348.37	600.00	1.8202

Non-zero binary interaction parameters:

	C1	C2	C3,IC4,C4,IC5,C5,C6,HC7,HC8,HC9,HC11,HC13, HC16,HC18,HC20,HC23,HC26,HC30,HC35,HC42,HC57
N2	0.020	0.060	0.080
CO2	0.120	0.150	0.150

Coefficients for Lohrenz-Bray-Clark viscosity correlation[12]

A0 = 0.1023000
A1 = 0.0233640
A2 = 0.0585330
A3 = -.0407580
A4 = 0.0121525

TABLE 6 - Flooding sequences.

Injection Fluid	Experiment 1		Experiment 2	
	Rate (cm^3/hr)	Amount (PV)	Rate (cm^3/hr)	Amount (PV)
Oil	8	0.5	9	1.2
Oil	205	0.6	200	0.7
Water	4	1.1	3	1.0
Gas	2.47	1.7	2.58	3.4

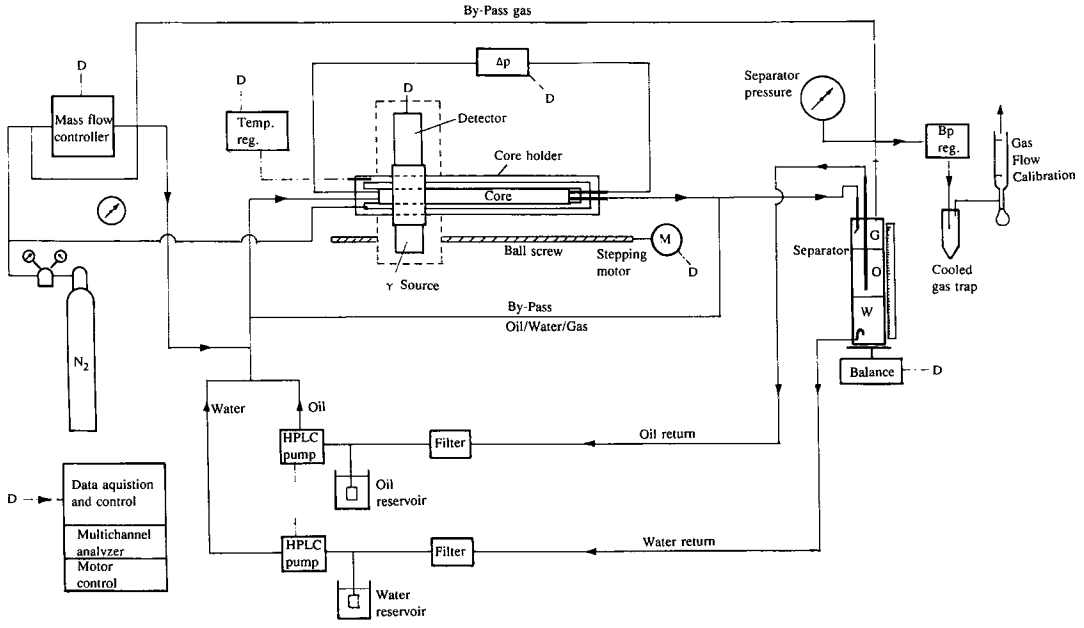

Fig. 1 - Apparatus for measurements of relative permeabilities.

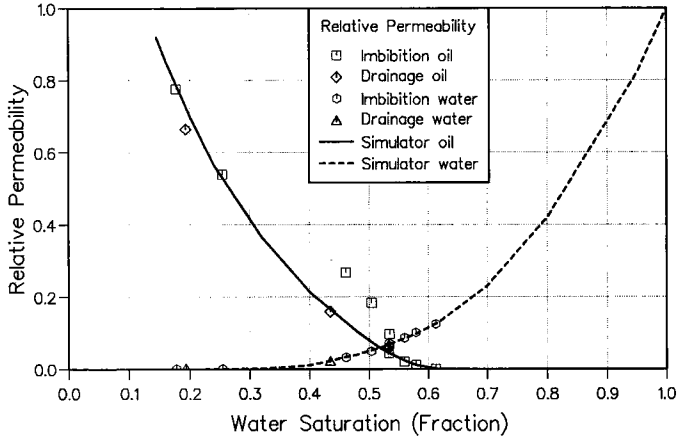

Fig. 2 - Oil - water relative permeabilities.

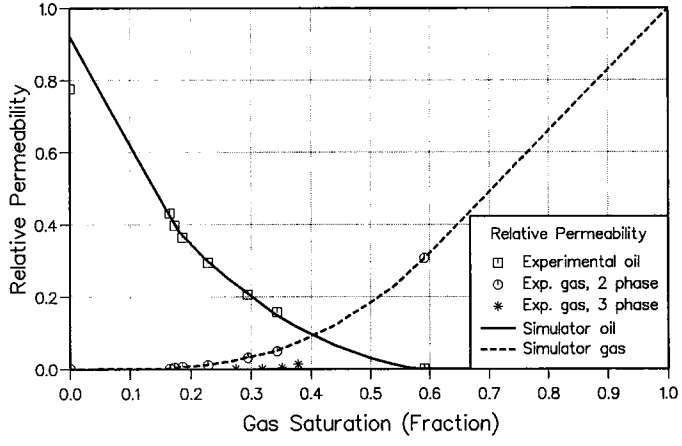

Fig. 3 - Gas - oil relative permeabilities.

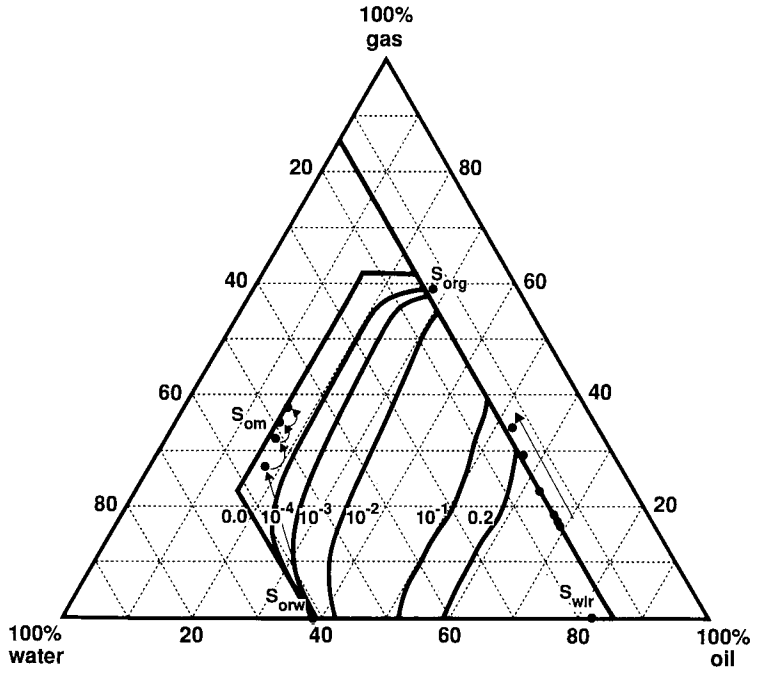

Fig. 4 - Rock curve oil isoperms and residual oil saturations.

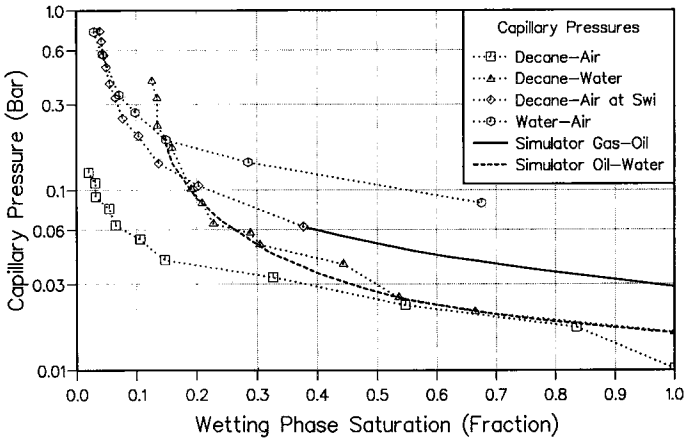

Fig. 5 - Experimental and rock curves for capillary pressures.

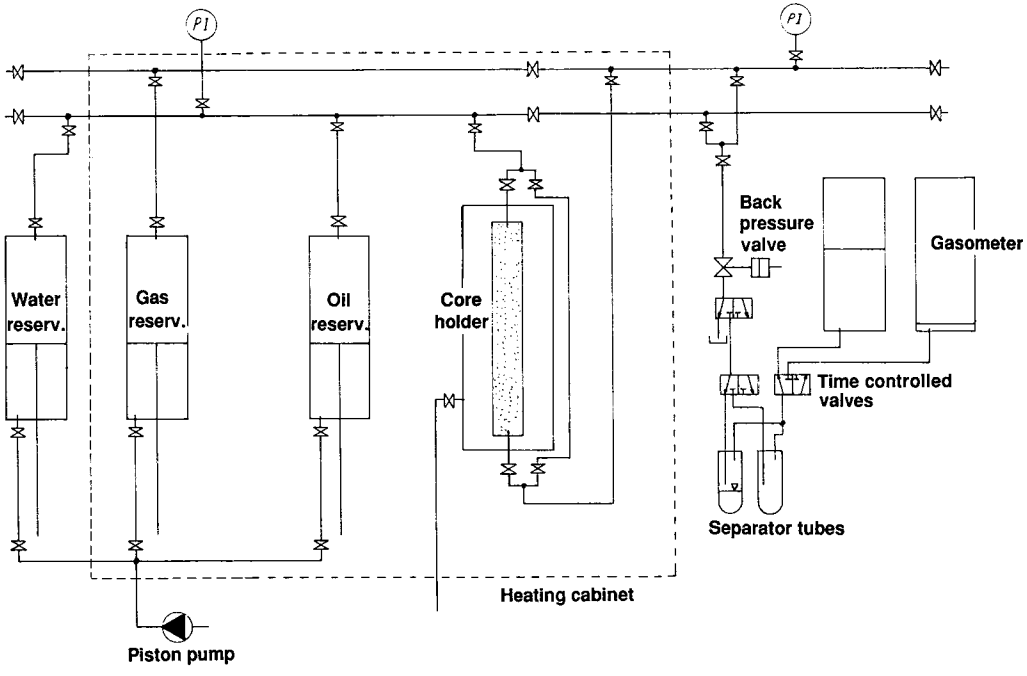

Fig. 6 - High pressure flooding apparatus.

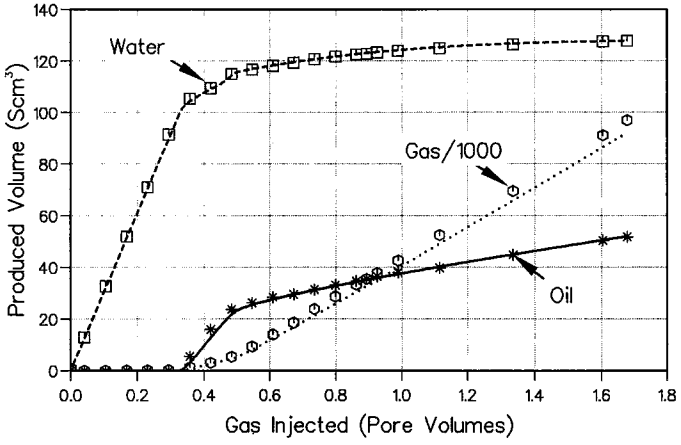

Fig. 7 - Simulated and experimental recoveries of Experiment 1.

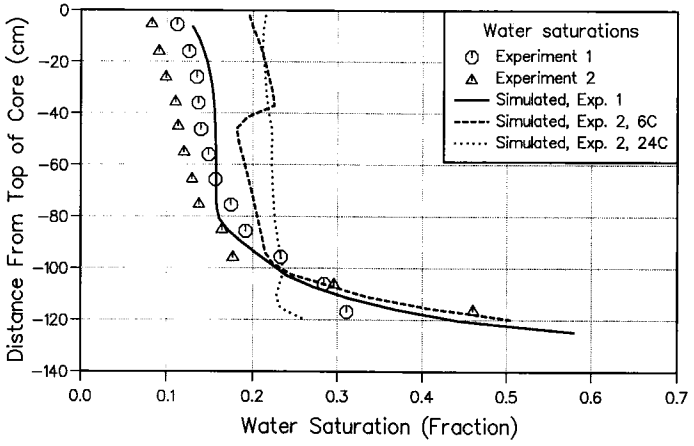

Fig. 8 - Simulated and experimental final water saturations of Experiments 1 and 2.

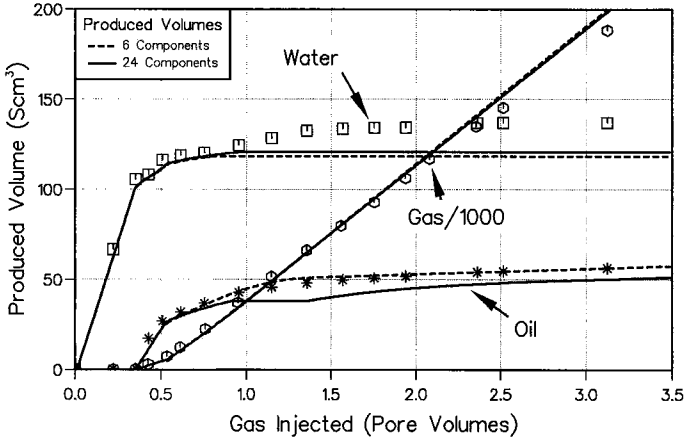

Fig. 9 - Simulated and experimental recoveries of Experiment 2.

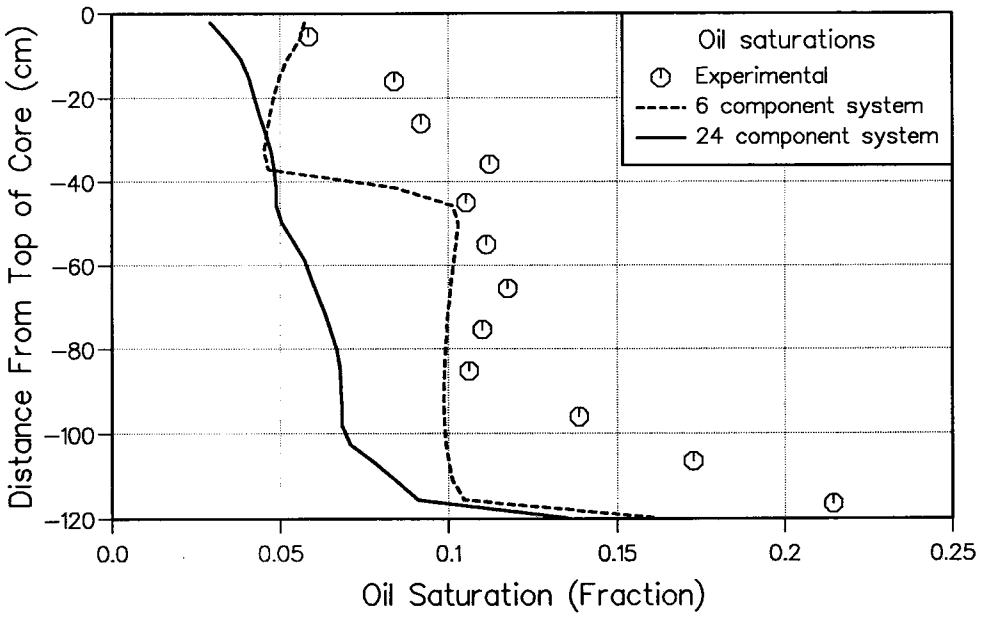

Fig. 10 - Simulated and experimentally estimated final oil saturations of Experiment 2.

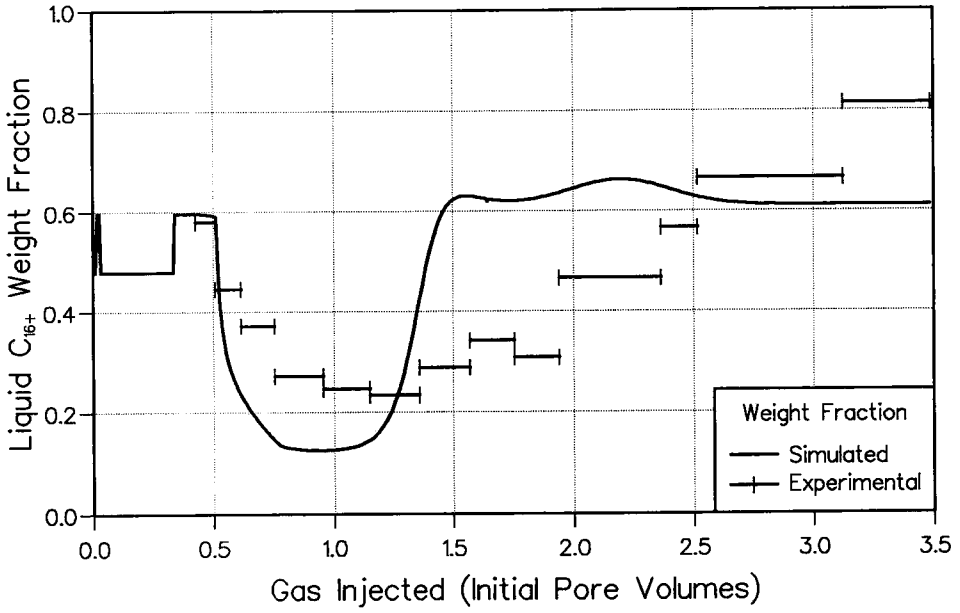

Fig. 11 - Simulated and experimental produced oil's C_{16+} fraction from Experiment 2.

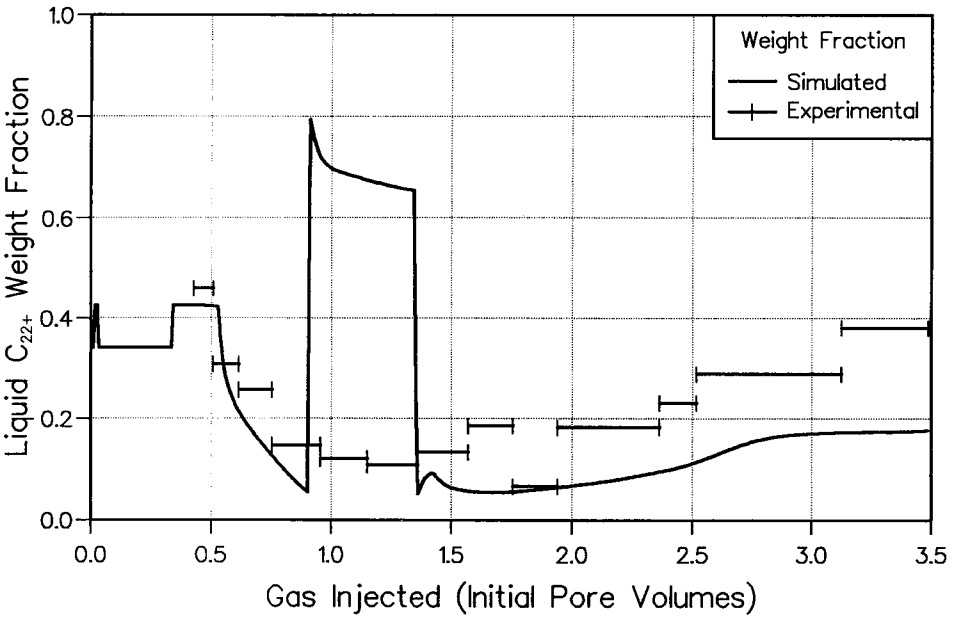

Fig. 12 - Simulated and experimental produced oil's C_{22+} fraction from Experiment 2.

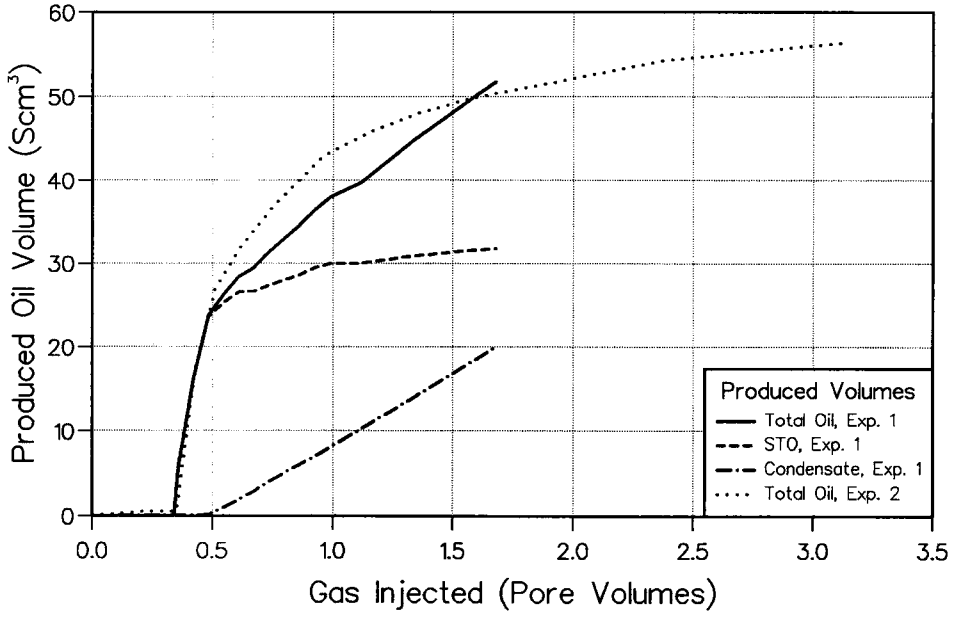

Fig. 13 - Experimental recoveries from Experiments 1 and 2.